Available online at www.sciencedirect.com
ScienceDirect
ELSEVIER
October 2012, 19(5): 45–50
www.sciencedirect.com/science/journal/10058885
The Journal of China Universities of Posts and Telecommunications
http://jcupt.xsw.bupt.cn

A cluster-based analysis of propagation characteristics in MIMO relay channels based on wideband measurement

NIE Xin[1,2] (✉), ZHANG Jian-hua[2], TIAN Lei[2], ZHANG Ping[2]

1. Beijing Institute of Spacecraft System Engineering, Beijing 100094, China
2. Wireless Technology Innovation Institute, Beijing University of Posts and Telecommunications, Beijing 100876, China

Abstract

In this paper, the characteristics of clusters induced by a variety of propagation mechanisms in the link from the relay station (RS) to the mobile station (MS) are presented. Based on the results of high resolution channel parameter estimation, an automatic framework integrated with the manual intervention is utilized to perform the cluster identification and tracking. The power proportion and angular spread of clusters are investigated in both the line-of-sight (LOS) and non-line-of-sight (NLOS) scenarios. The measurement results indicate that the channel characteristics of clusters are different from the link from the base station to the MS due to the lower height of the RS antennas.

Keywords relay, wideband channel measurement, cluster statistics, propagation mechanism

1 Introduction

The development of multiple-input multiple-output (MIMO) relay systems demands the accurate knowledge of the propagation effects. Thorough understanding and reasonable modeling of channel characteristics are essential for algorithm development and performance evaluation. An important feature of the propagation channel with respect to MIMO applications is that the multipath components (MPCs) are concentrated in clusters that correspond to scatterers in the environment. The MPCs in a cluster stem from the same propagation mechanism, and are described by similar parameters, i.e., delay, angle of arrival (AOA), and angle of departure (AOD) [1]. A number of state-of-the-art channel models (COST273, SCM/SCME, etc.) have been developed relying on the physical phenomena of the cluster. Recently, the cluster identification and channel statistics in the cluster have been discussed in several papers. The performance comparison of clustering methods was addressed by [2]. The cluster statistics in the indoor hotspot and office scenarios were quantified in Refs. [3–4] separately. However, antennas of the RS are typically much lower than those of the conventional base station (BS) to reduce operating and maintenance costs [5]. Because of the lower height of the RS antennas, the surroundings of the wireless link from the RS to the MS is quite different from that of the link from the BS to the MS. The cluster statistics in the relay scenario were not reported in the literature yet.

In this paper, wideband channel measurements were conducted in an urban area in Beijing, China to investigate the channel statistics the cluster and corresponding propagation mechanisms. The measurement area is characterized by high building density, which makes it necessary to employ the relay to enhance the coverage in the shadowed area. From the outcomes of the channel parameter estimation, the cluster identification and tracking are performed. The channel statistics in cluster, including the power proportion (PP), angular spread of departure (ASD) and angular spread of arrival (ASA), are presented based on the tracking results. The propagation mechanisms are also investigated.

Received date: 10-03-2012
Corresponding author: NIE Xin, E-mail: niexin.bupt@gmail.com
DOI: 10.1016/S1005-8885(11)60299-9

2 Measurement equipments and environment

The measurements were conducted at the center frequency of 2.35 GHz with the bandwidth of 50 MHz, which is within the frequency band allocated to the IMT-Advanced systems. The transmitting power at the antenna input is 26 dBm. The Elektrobit Propsound channel sounder was employed, which is described in detail in Ref. [6]. The sounder works in a time-division multiplexing mode. Periodic pseudo random binary signals with the code length of 255 chips are transmitted between different sub-channels. The interval within which all sub-channels are sounded once is referred to as a measurement cycle. The 3D cylinderal omni-directional array, which consists of 56 dual-polarized patch elements, was utilized at both the RS and the MS. One ring of the elements were selected as the active antenna, i.e., 8 dual-polarized patch elements. The antenna pattern was obtained from Satimo SG128 antenna measurement system.

The measurement scenario is illustrated in Fig. 1. The star mark indicates the position of the RS. The solid line denotes the LOS measurement route, while the dash line denotes the NLOS measurement route. The arrow shows the movement direction of the MS.

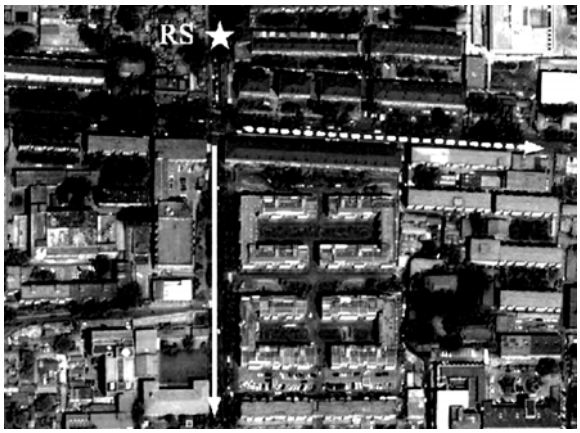

Fig. 1 Vertical view of measurement scenario

During the measurements, the RS antennas were placed on a testing vehicle around 7 m above the street. Antennas of the MS were mounted on a trolley. The height of MS antennas was adjusted to about 1.8 m in order to imitate the height of human body. Continuous routes were measured in both the LOS and the NLOS scenarios by moving the MS. The positions of the MS were recorded by global positioning system (GPS). The GPS data sets were fitted to the map and interpolated to mitigate the inaccuracy. Three local areas (LAs) are selected in each measurement route. The LA is defined as the circular range with a radius of 20 times of the wavelength. The distance from the RS to the center of LA. #1, #2, and #3 are 50 m, 150 m and 250 m, respectively.

3 Data post-processing

The data post-processing consists of two procedures: estimating the parameter set describing the individual MPC, grouping the MPCs into clusters and tracking the evolution of the clusters.

3.1 Parameter estimation

After the channel impulse response (CIR) is obtained, the noise-cut is performed first to ensure that the signal is much stronger than the noise so that the additive noise does not affect the inherent characteristic of the channel. Since the noise level P_{n} varies with time, the noise level estimation is done for each measurement cycle. A threshold P_{t} is then determined by both the estimated noise level P_{n} and the peak power of CIRs P_{p}, i.e., $P_{\mathrm{t}} = \max\left\{P_{\mathrm{n}} + D_{\mathrm{m}}, P_{\mathrm{p}} - D_{\mathrm{r}}\right\}$, where D_{m} is the noise margin from noise floor P_{n} and D_{r} denotes the dynamic range from the peak power P_{p}. MPCs with power below the threshold P_{t} are ignored. The dynamic range D_{r} is set to 25 dB and the margin D_{m} is set to 6 dB.

The wideband channel can be described as the superposition of L MPCs, which are characterized by a parameter set $\Theta \doteq \left\{(\Omega_{1,\ell}, \Omega_{2,\ell}, \tau_\ell, \nu_\ell, \alpha_\ell), \ell = 1, 2, ..., L\right\}$. $\Omega_{1,\ell}$, $\Omega_{2,\ell}$, τ_ℓ, ν_ℓ, α_ℓ denote, respectively, the AOD, the AOA, the propagation delay, the Doppler shift and the complex amplitude of the ℓth MPC. The space-alternating generalized expectation-maximization (SAGE) [7] is utilized to estimate the parameter set Θ from the measured CIRs. The MPCs with the power $|\alpha_\ell|^2$ less than 1% of the total power $\sum_{\ell=1}^{L}|\alpha_\ell|^2$ are removed from the MPC set since they do not contribute significantly. The parameter sets of 550 spatial positions are estimated in each measurement route.

3.2 Cluster identification and tracking

The KPowerMeans algorithm [8] is chosen as the

clustering algorithm. The KPowerMeans algorithm provides joint multi-dimensional clustering of MPCs according to the parameter set θ, and iteratively minimizes the total sum of power-weighted distances of each MPC to its associated cluster centroid based on the multipath component distance (MCD). The MCD d between the ith and jth MPC is given by $d_{ij}=\sqrt{\left\|d_{1,ij}\right\|+\left\|d_{2,ij}\right\|+d_{\tau,ij}^2}$, where $d_{g,ij}$, $g\in\{1,2\}$, $1\leqslant i, j\leqslant L$ is the distance brought about by the angular difference, $\|\cdot\|$ is the norm operator. The $d_{g,ij}$ is obtained as

$$d_{g,ij}=\frac{1}{2}\left|\begin{pmatrix}\sin\Omega_{g,i}\\ \cos\Omega_{g,i}\end{pmatrix}-\begin{pmatrix}\sin\Omega_{g,j}\\ \cos\Omega_{g,j}\end{pmatrix}\right| \tag{1}$$

$d_{\tau,ij}$, $1\leqslant i, j\leqslant L$ is the delay distance, which can be calculated as $d_{\tau,ij}=|\tau_i-\tau_j|\tau_{\text{std}}$ with $\Delta\tau_{\max}=\max_{i,j}\{|\tau_i-\tau_j|\}$, τ_{std} being the standard deviation of the delay.

Two validity indices are selected to jointly determine the optimal number of clusters, namely, the Calinski-Harabasz (CH) [8] and kim-parks (KP) [9] index. The CH index corresponds to the ratio between the traces of the between-cluster scatter matrix and the within-cluster scatter matrix. Using the KP index, the optimal cluster number K_{KP} is taken from K candidate numbers by

$$K_{\text{KP}}=\underset{K}{\operatorname{argmin}}\left\{\frac{1}{K}\sum_k S_k+\frac{K}{\underset{k\neq k'}{\arg\min}[d(u_k,u_{k'})]}\right\} \tag{2}$$

where S_k, $1\leqslant k\leqslant K$ is a measurement of the compactness in one cluster, and the u_k and $u_{k'}$ are the centroids of the kth and k'th cluster, respectively.

An example of the cluster identification is shown in Fig. 2, The MPCs are grouped in the AOA-AOD-delay domain.

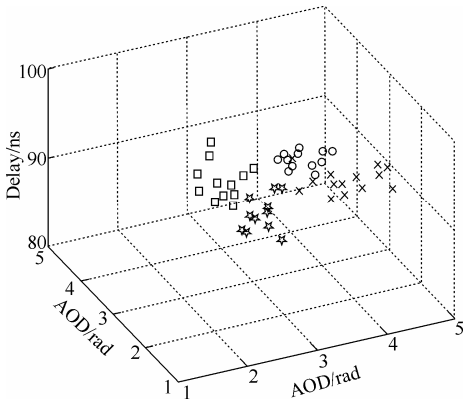

Fig. 2 Clustering result of one measurement cycle in the NLOS scenario

Based on the results of cluster identification, the automatic cluster tracking framework proposed in Ref. [10] is adopted to investigate the change trends of the clusters. The tracking is based on the distance matrix $\boldsymbol{D}$, whose element is calculated as $\boldsymbol{D}_{ij}=\text{MCD}\left(u_M^{\text{old}},u_N^{\text{new}}\right)$, where u_M^{old} is the Mth old centroid and u_N^{new} is the Nth new centroid. Further details about the tracking framework can be found in Ref. [8]. The main deficiency of the automatic framework is the lack of physical realism. The cluster tracking is carried out irrespective of the real-world scatterers and correspo- nding propagation mechanisms. Thus, the visual identification and manual intervention are added to the automatic tracking framework in our analysis. First, the scatterers are located according to the angle and delay information of the cluster centroids. The propagation mechanism is also found out. Then, the clusters appearing in different measurement cycles created by the identical scatterer are regarded as the same cluster evolving over the time.

4 Results and discussion

4.1 Power proportion of clusters

The PP trends of clusters introduced by various propagation mechanisms in the LOS scenario are shown in Fig. 3.

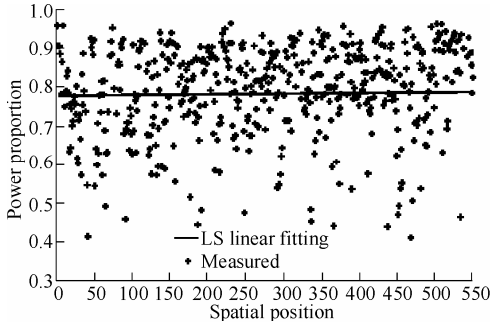

(a) PP of the LOS propagation

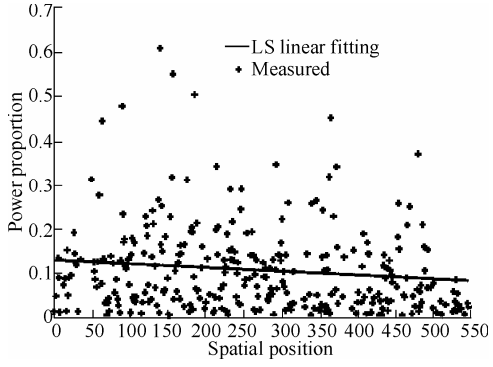

(b) PP of the FO reflection

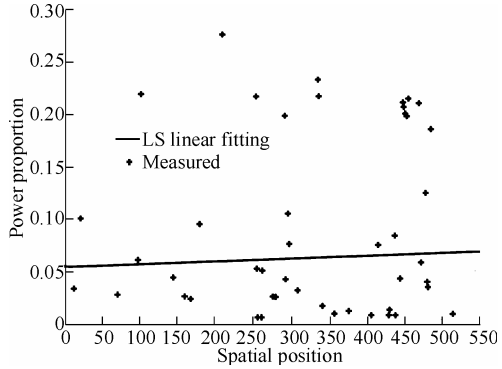

(c) PP of the HO reflection

Fig. 3 The trend of the PP caused by different propagation mechanisms in the LOS scenario, as a function of the spatial position

In the figure, the horizontal axis represents the distance from the MS to the RS in meters，and the points on the vertical axis correspond to the PP of clusters caused by different propagation mechanisms. It can be seen that the LOS propagation, the first-order (FO) and high-order (HO) reflection are the main propagation mechanisms (The reflection order refers to the number of reflections that the MPC goes through before it reaches the receiver). The reflection is mainly induced by the buildings on both sides of the street. From the comparison of Figs. 3(a), 3(b) and 3(c), it can seen that the LOS propagation is dominate in the whole region, and the ratio to the total power is about 80%. The power of the FO and HO reflection accounts approximately for 10% and 5% of the total power. It can also be found that the PP of different mechanisms basically remains constant.

The trends of PP for different propagation mechanisms are shown in Fig. 4. The meaning of coordinate axes in Fig. 4 is the same as that of the coordinate axes in Fig. 3. Compared to the LOS scenario, the signal arrives at the MS in a more complicated way in the NLOS scenario. When the MS is in LA. #1, there are mainly three ways in which the signal travels to the MS, namely, the FO reflection, the HO reflection and the diffraction (DF) over the rooftop. The FO reflection contributes the largest part (about 40%) to the total power. As the MS moves apart from the RS, a new way of signal propagation occurs. In this way, the signal impinges on the buildings on the side of the street through the diffraction over the rooftop), and then reflects to the MS. This kind of propagation is referred to as the reflection after diffraction (RD) propagation below. When the MS reaches LA. #3, the signal cannot travel to the MS via the FO reflection due to the geometry of the street. The DF is also blocked by the building near the RS. Thus, the HO reflection and the RD propagation become the primary propagation mechanisms. The power contributed by the HO and RD propagation accounts for more than 90% of the total power. In general, the PP of the HO reflection and RD propagation increase as the MS moves away from the RS. On the other hand, the PP introduced by the FO reflection and DF decreases. It also can be concluded from the above results that the signal traveling from the RS to the MS is seriously influenced by the local scatterers of the RS side due to the lower height of the RS antennas in the NLOS scenario.

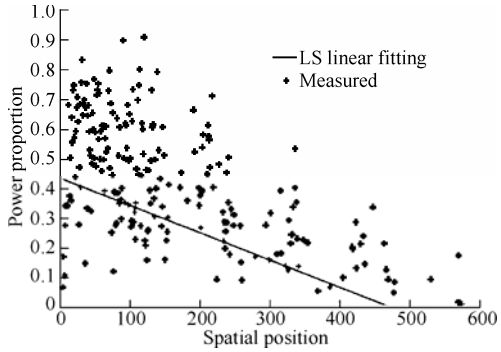

(a) PP of the FO propagation

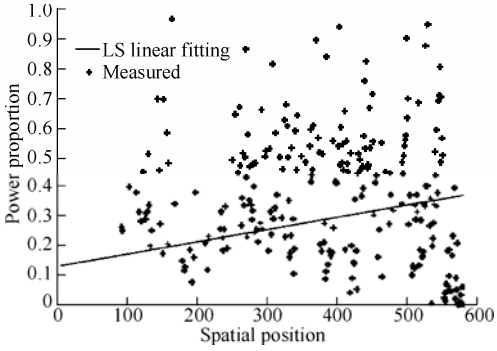

(b) PP of the HO reflection

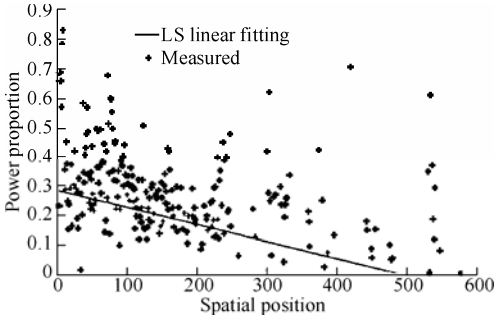

(c) PP of the DF propagation

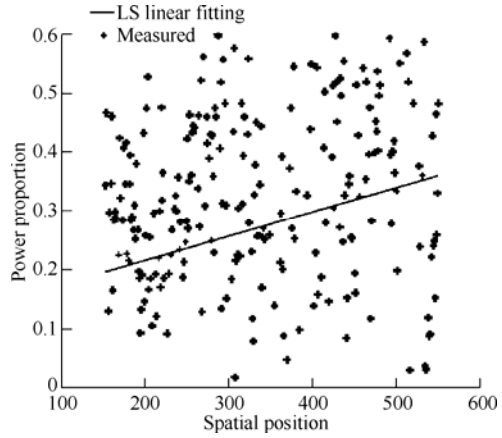

(d) PP of the RD propagation

Fig. 4 The trend of the PP caused by different propagation mechanisms in the NLOS scenario, as a function of the spatial position

The results provide a thorough understanding of the propagation mechanism in the link between the RS and the MS in both LOS and NLOS scenarios. The number and PP of the clusters, which have not been reported in previous literature, can be adopted in the channel model based on clusters. Combined with the measured data of angular spread given below, the statistics of the clusters constitute the basis for the channel model in spatial domain.

4.2 Angular spread in the cluster

The AS in the *k*th cluster can be calculated using the method proposed in Ref. [11]. The dominate clusters and corresponding mean ASs in three LAs in the LOS scenario are listed in Table 1.

Table 1 ASs in different LAs in the LOS scenario

LA.	Cluster No.	ASA/ (°)	ASD/ (°)	Mechanism
#1	C1	8.8	8.0	LOS
	C2	14.7	8.6	FO
	C3	16.8	8.4	HO
#2	C1	9.2	7.7	LOS
	C2	14.2	6.9	FO
	C3	15.2	7.6	HO
#3	C1	7.2	6.8	LOS
	C2	10.3	7.6	FO
	C3	11.7	7.0	HO

The total power of the listed clusters exceeds 90% of the total power. From Table 1, it can be found the LOS cluster manifests the smallest ASA. Meanwhile, the ASA in the cluster induced by the HO reflection is the largest. The maximum difference is 8°. The results indicate that the ASA in the cluster increases as the reflection order increases. It also can be observed that the ASA of FO and HO reflection reduces as the distance from the RS to the MS becomes larger. This is mainly because the MPCs attenuate more after traveling for longer distance and undergoing more interaction with the scatterers. Only the MPCs with stronger power survive. Due to the street canyon effect, the MPCs become more concentrated. The ASD in the cluster is smaller compared with the ASA. Besides, the ASD shows less variation. The maximum difference is only 1.6°. Table 2 gives the mean ASs in the cluster for the NLOS case. The ASA and ASD in the NLOS scenario show similar relation with those in the LOS scenario, that is, the ASD is smaller than the ASA. The ASs are larger than those in the LOS scenario owning to the increment of scatterers in the NLOS scenario. For the same reason, the ASs of clusters introduced by different propagation mechanisms have little difference. The ASA and ASD in the cluster are found to be 5.3° and 5.3° in the outdoor environment in the conventional link from the BS to the MS [12]. The ASs in the cluster in the link from the RS to the MS are larger because of the more complex scattering environment. Based on the results shown in Tables 1 and 2, a conclusion can be drawn that both the number of clusters and the statistics of ASs in clusters change with the distance between the RS and the MS. As a result, the channel model with invariant parameters, regardless of the coverage of the RS, reduces the accuracy of performance evaluation. The numerical results, which are the measurement of spatial statistics in the relay channel, can provide relevant parameters for the channel model according to the coverage of the RS.

Table 2 ASs in different LAs in the NLOS scenario

LA.	Cluster No.	ASA/ (°)	ASD/ (°)	Mechanism
#1	C1	15.9	12.5	DF
	C2	13.6	13.4	FO
	C3	14.6	14.5	HO
#2	C1	15.1	10.9	DF
	C2	15.9	12.2	FO
	C3	14.0	13.0	HO
	C4	15.3	12.3	RD
#3	C1	16.9	13.0	HO
	C2	16.0	12.6	RD

5 Conclusions

In this paper, the ASs in the cluster are studied based on the outdoor wideband measurement in a typical scenario of relay application. The results indicate that, in the LOS scenario, the ASA in the clusters caused by the FO and HO reflection increases as the reflection order increases, and decreases as the distance from the RS to the MS becomes

larger. Meanwhile, the ASD in the cluster is smaller and shows less variation compared with the ASA. In the NLOS scenario, the ASs are larger than those in the LOS scenario owning to the increment of scatterers. The ASs of clusters introduced by different propagation mechanisms have little difference. The PP of clusters is also investigated. The LOS propagation, which accounts for more than 80% of the total received power, is dominant in the whole area of the LOS scenario. The signal travels in a more complicated way in the NLOS scenario. The FO and HO reflection, as well as the DF and RD propagation, are all important propagation mechanisms. Generally, the PP of the HO reflection and RD propagation increases as the MS moves away from the RS. Due to the lower height of the RS antennas, the local scatterers of the RS side affect the way of signal propagation significantly, which makes the characteristics of clusters different from those in the link from the BS to the MS. As a result, the validity of channel model reduces if the channel parameters obtained from the link from the BS to the MS are directly applied to the link between the RS and the MS. The number and PP of the clusters, as well as the ASs in clusters, can be adopted in the relay channel model based on clusters. Taking into consideration the relationship between the channel parameters and the coverage of the RS can further improve the accuracy of performance evaluation

Acknowledgements

The work was supported by China National Science and Technology Major Project (2009ZX03007-003), the Hi-Tech Research and Development Programm of China (2009AA011502).

References

1. Toeltsch M, Laurila J, Kalliola K, et al. Statistical characterization of urban spatial radio channels. IEEE Journal on Selected Areas in Communications, 2002, 20(3): 539–549
2. Schneider C, Bauer M, Narandzic M, et al. Clustering of MIMO channel parameters–Performance comparison. Proceedings of the 69th IEEE Vehicular Technology Conference (VTC-Spring'09), Apr 26–29, 2009, Barcelona, Spain. Piscataway, NJ, USA: IEEE, 2009: 5p
3. Huang C, Zhang J H, Nie X, et al. Cluster characteristics of wideband MIMO channel in indoor hotspot scenario at 2.35 GHz. Proceedings of the 70th IEEE Vehicular Technology Conference (VTC-Fall'09), Sep 20–23, 2009, Anchorage, AK, USA. Piscataway, NJ, USA: IEEE, 2009: 5p
4. Czink N, Yin X F, Ozcelik H, et al. Cluster characteristics in a MIMO indoor propagation environment. IEEE Transactions on Wireless Communications, 2007, 6(4):1465–475
5. Pabst R, Walke B, Schultz D, et al. Relay-based deployment concepts for wireless and mobile broadband radio. IEEE Communications Magazine, 2004, 42(9): 80–89
6. Chung H K, Vloeberghs N, Kwon H K, et al. MIMO channel sounder implementation and effects of sounder impairment on statistics of multipath delay spread. Proceedings of the 62nd IEEE Vehicular Technology Conference (VTC-Fall'05): Vol 1, Sep 26–29, 2004, Dallas, TX, USA. Piscataway, NJ, USA: IEEE, 2005: 349–353
7. Fleury B, Tschudin M, Heddergott R, et al. Channel parameter estimation in mobile radio environments using the SAGE algorithm. IEEE Journal on Selected Areas in Communications, 1999, 17(3): 434–450
8. Czink N, Cera P, Salo J, et al. A framework for automatic clustering of parametric MIMO channel data including path powers. Proceedings of the 64th IEEE Vehicular Technology Conference (VTC-Fall'06), Sep 25–28, 2006, Montreal, Canada. Piscataway, NJ, USA: IEEE, 2006: 5p
9. Kim D J, Park Y W, Park D J. A novel validity index for determination of the optimal number of clusters. IEICE Transactions on Information and Systems, 2001, E84(2): 281–285
10. Czink N, Mecklenbrauker C, Galdo G. A novel automatic cluster tracking algorithm. Proceedings of the 17th IEEE International Symposium on Personal, Indoor and Mobile Radio Communications (PIMRC'06), Sep 11–14, 2006, Helsinki, Finland. Piscataway, NJ, USA: IEEE, 2006: 5p
11. 3GPP TR 25.996 v7.0.0. Spatial channel model for multiple input multiple output (MIMO) simulations. 2007
12. Dong W, Zhang J H, Gao X, et al. Cluster identification and properties of outdoor wideband MIMO channel. Proceedings of the 66th IEEE Vehicular Technology Conference (VTC-Fall'07), Sep 30–Oct 3, 2007, Baltimore, MD, USA. Piscataway , NJ, USA: IEEE, 2007: 829–833

(Editor: ZHANG Ying)